Acquiring Scattering Properties of Participating Media by Dilution

Srinivasa G. Narasimhan[1], Mohit Gupta[1], Craig Donner[2], Ravi Ramamoorthi[3], Shree K. Nayar[3], Henrik Wann Jensen[2]

[1]Carnegie Mellon University*   [2]University of California, San Diego   [3]Columbia University

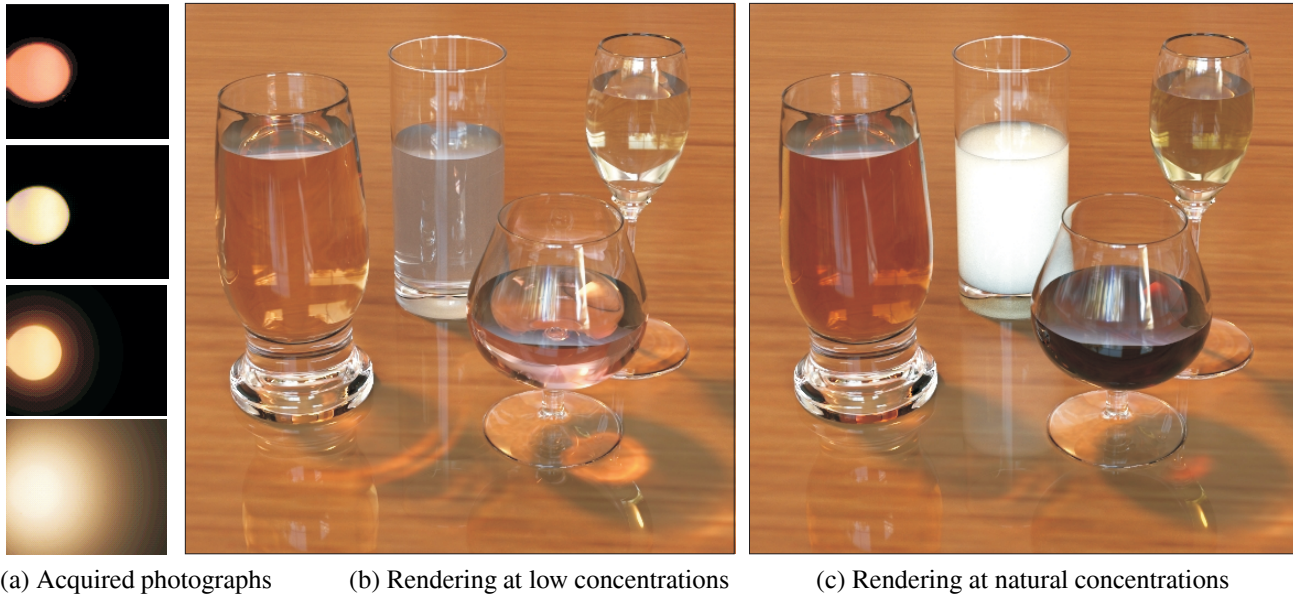| (a) Acquired photographs | (b) Rendering at low concentrations | (c) Rendering at natural concentrations |

Figure 1: *(a) Photographs of our simple setup consisting of a glass tank and a bulb, filled with diluted participating media (from top, MERLOT, CHARDON-NAY, YUENGLING beer and milk). The colors of the bulb and the glow around it illustrate the scattering and absorption properties in these media. At low concentrations, single scattering of light is dominant while multiple scattering of light is negligible. From a single HDR photograph, we robustly estimate all the scattering properties of the medium. Once these properties are estimated, a standard volumetric Monte Carlo technique can be used to create renderings at any concentration and with multiple scattering, as shown in (b) and (c). While the colors are only slightly visible in the diluted setting in (b), notice the bright colors of the liquids - deep red and golden-yellow wines, soft white milk, and orange-red beer - in their natural concentrations. Notice, also the differences in the caustics and the strong interreflections of milk onto other liquids.*

Abstract

The visual world around us displays a rich set of volumetric effects due to participating media. The appearance of these media is governed by several physical properties such as particle densities, shapes and sizes, which must be input (directly or indirectly) to a rendering algorithm to generate realistic images. While there has been significant progress in developing rendering techniques (for instance, volumetric Monte Carlo methods and analytic approximations), there are very few methods that measure or estimate these properties for media that are of relevance to computer graphics. In this paper, we present a simple device and technique for robustly estimating the properties of a broad class of participating media that can be either (a) diluted in water such as juices, beverages, paints and cleaning supplies, or (b) dissolved in water such as powders and sugar/salt crystals, or (c) suspended in water such as impurities. The key idea is to dilute the concentrations of the media so that single scattering effects dominate and multiple scattering becomes negligible, leading to a simple and robust estimation algorithm. Furthermore, unlike previous approaches that require complicated or separate measurement setups for different types or properties of media, our method and setup can be used to measure media with a complete range of absorption and scattering properties from a single HDR photograph. Once the parameters of the diluted medium are estimated, a volumetric Monte Carlo technique may be used to create renderings of any medium concentration and with multiple scattering. We have measured the scattering parameters of forty commonly found materials, that can be immediately used by the computer graphics community. We can also create realistic images of combinations or mixtures of the original measured materials, thus giving the user a wide flexibility in making realistic images of participating media.

*e-mail:srinivas@cs.cmu.edu

1 Introduction

Very often in our daily lives, we see participating media such as fluids (juices, beverages, milks) and underwater impurities (natural ocean, river and lake waters). The propagation of light through these media results in a broad range of effects, including softer appearance of milk, coloring of wines and juices, the transformation of appearances when liquids are mixed (coffee with milk, and cocktails), the brilliant caustics from glasses containing these liquids, and low visibility in underwater situations. These effects inherently depend on several physical properties of the media such as

scattering nature, sizes, shapes, and densities of particles [Hulst 1957; Chandrasekhar 1960]. Rendering these effects accurately is critical to achieving photo-realism in computer graphics.

In the past few years, there has been a considerable effort towards developing efficient and accurate rendering algorithms for participating media, based on Monte Carlo simulation and analytic approximations. All these algorithms and models contain parameters (scattering coefficient, absorption coefficient, phase function) that directly or indirectly represent the physical properties of the medium. In order to faithfully render the effects of any participating medium, the right parameters must be input. Given the progress in developing rendering algorithms, the quality of images is now often limited by the quality of these input parameters. Since there has so far been relatively little work in measuring or estimating scattering properties of media relevant to computer graphics, the parameters are currently often set in an ad-hoc manner.

This situation is similar in some ways to that of standard surface rendering. In that case, global illumination algorithms have progressed to the point of creating almost photo-realistic images, leaving the realism limited by the quality of the reflectance models, and leading to much recent effort on measuring BRDFs. [Marschner 1998; Dana et al. 1997; Matusik et al. 2003]. However, existing methods for directly measuring physical properties for media usually require very expensive equipment, such as the particle sizing apparatus used in colloidal chemistry [Finsy and Joosten 1991; Jaeger et al. 1991], resulting in little usable data for graphics.

Earlier efforts to estimate scattering properties from images of media have often yielded ill-conditioned and non-unique results, because of the difficulties of solving the inverse light transport problem. The reasoning for the ill-conditioning of the inverse problem is mainly due to multiple scattering, which blurs the incident light field and results in significant loss of information [McCormick 1981; McCormick 1985; Antyufeev 2000]. This is analogous to the ill-conditioning of BRDF estimation under complex illumination [Ramamoorthi and Hanrahan 2001]. In this paper, we take a completely different approach. The key idea is to estimate properties of media by acquiring the data in a state where multiple scattering effects are negligible. Instead, the data is acquired when single scattering (which does not degrade the incident light significantly) is the dominant effect. This is achieved by diluting the material to low concentrations.

We present a simple and inexpensive experimental setup, along with a robust and accurate technique for measuring the scattering properties of a broad class of participating media that can be either (a) diluted in water such as juices, beverages, paints and cleaning supplies, or (b) suspended in natural waters such as impurities and organisms, or even (c) dissolved in water such as powders and sugar or salt crystals. These media collectively have a wide range of scattering and absorption properties. We first derive a simple image formation model for single scattering of light in our setup. Through extensive simulations of both our model and ground truth (with multiple scattering), we then determine the space of concentrations and scattering properties of media for which single scattering is dominant. Within this regime of valid concentrations, we conduct simulations to demonstrate that our estimation technique uniquely solves the inverse single scattering light transport problem. Finally, we present a simple experimental procedure to determine the best concentration (dilution) for any material despite no prior knowledge of its scattering properties.

We have used our approach to create a dataset of scattering parameters for **forty commonly found materials**, which can be directly used for computer graphics rendering. Once the scattering parameters have been estimated, they can be used to render realistic images of arbitrary concentrations of the material with multiple scattering, using a standard physically based volumetric rendering algorithm. Figure 1 shows two renderings of a scene with four

Medium Property	Notation
Concentration or Volume Fraction	C
Scattering Coefficient (mm^{-1})	β
Absorption Coefficient (mm^{-1})	κ
Extinction Coefficient (mm^{-1})	$\sigma = \beta + \kappa$
Single Scattering Albedo	$\omega = \beta/\sigma$
Scattering Angle	θ
Henyey-Greenstein (H-G) Parameter	g
H-G Phase Function	$P(g,\theta) = \frac{1}{4\pi} \frac{1-g^2}{(1+g^2-2g\cos\theta)^{3/2}}$

Figure 2: *The different scattering properties of a participating medium and their notations used in this paper. Light transport equations are usually written in terms of three parameters σ, β and g. We estimate these parameters for participating media based on single scattering.*

liquids in their natural high density states and their diluted states. The scattering parameters of each material were computed using a single HDR photograph of our setup. Notice the bright saturated colors obtained despite the murky appearance of the diluted states. We can also create realistic images of mixtures of the original measured materials, thus giving the user a wide flexibility in creating realistic images of participating media.

2 Related Work

Figure 2 shows the most common properties of participating media including the scattering and absorption coefficients, and the phase function (angular scattering distribution represented by the Henyey-Greenstein (H-G) model [Henyey and Greenstein 1941]). The scattering and absorption coefficients are proportional to the concentration or volume fraction of the particulate medium. We will briefly review some of the representative works on the direct measurement and indirect estimation of these parameters.

Estimation based on analytic approximations to light transport. Surprisingly, little work has been done in computer graphics on the measurement of scattering properties of media. A recent work is that of [Jensen et al. 2001], on the diffusion model for subsurface scattering. They present a measurement of a number of translucent materials. However, the diffusion approximation assumes multiple scattering for optically dense media, so that only a limited amount of information on the scattering parameters can be estimated. For instance, this approximation is independent of the phase function of the medium, and therefore this important property cannot be estimated. Furthermore, the diffusion is a poor approximation when scattering is comparable to absorption [Prahl 1988]. The analytic multiple scattering model presented in [Narasimhan and Nayar 2003] has also been used to estimate properties of only purely scattering media (visibility and type of weather such as fog and mist). Our focus is somewhat different in considering fluids like juices or beverages, instead of subsurface scattering in translucent solids like marble and skin, or weather conditions such as fog. Nevertheless, our approach is valid for media with the entire range of absorbing and scattering properties, significantly extending the class of measurable media for graphics.

Most recently, Hawkins et. al., [2005] measure the extinction coefficient of optically thin smoke from the exponential attenuation of a laser beam in a tank. They also use a separate mirror setup to directly measure the phase function (see below). In contrast, our setup uses divergent beams from a simple bulb to include more light in the volume (than a single laser beam) for robust measurements, and requires only a single photograph to measure all scattering properties shown in Figure 2.

Numerical solution to inverse light transport: In cases where there are no analytic solutions to light transport, several works have taken a numerical approach to estimate scattering properties [McCormick 1996; Antyufeev 2000]. However, it is widely

known, that inverse problems in radiative transfer that take into account multiple scattering are ill-conditioned and require regularizing assumptions to obtain reliable estimates. See the reports and critiques by McCormick et al [1981; 1985]. Furthermore, the computational complexity of such inverse estimation techniques make it hard for measuring large sets of media for computer graphics or vision applications. Our focus here is on estimating scattering properties of media that can be measured in a state where multiple scattering is negligible.

The observation that single scattering is dominant for optically thin media has been made by [Hawkins et al. 2005; Sun et al. 2005]. We exploit this observation and apply the single scattering model for the first time to a large class of materials which exhibit significant multiple scattering in their natural states of existence. We also determine the exact range of optical thicknesses for which single scattering is dominant for media with arbitrary scattering properties, and propose an experimental procedure to ensure the dominance of single scattering in real data.

Goniophotometry is often used to directly measure the phase function. Here, several detectors measure radiance in different directions after being scattered by a very small volume of the medium. [Fuchs and Jaffe 2002] use thin laser light sheet microscopy for detecting and localizing microorganisms in ocean waters. [Boss and Pegau 2001; Oishi 1990] investigate the relationship of light scattering at a single angle and the extinction coefficient using specialized receivers and transmitters. However, all these techniques assume that there is no attenuation of light through the sample and require expensive devices with precise alignment of detectors and transmitters. In contrast, our setup is extremely simple (consisting of a glass tank and an off the shelf bulb), and our technique robustly estimates all properties from only a single photograph, thus making it inexpensive and easy to measure a large number of participating media.

3 Single Scattering in Dilute Media

Our approach is to measure media in a state where single scattering is dominant and multiple scattering is negligible. This is achieved by diluting the otherwise optically thick media, such as fluids, in water. The process of dilution does not usually corrupt the inherent scattering properties of media[1] since the scattering and absorption of pure water itself is negligible for very small distances (less than 50 cm) [Sullivan 1963]. We begin by presenting our acquisition setup and an image formation model for single scattered light transport within the measurement volume. We will then present extensive simulations of this model and compare with traditional Monte-Carlo approaches that include multiple scattering, to derive a valid space of scattering parameters over which single scattering is dominant. Based on this simulation, we design a simple experimental procedure to choose the best concentration for any particular medium. Later, we will describe our algorithm to estimate the scattering parameters using our image formation model.

3.1 Acquisition Setup

The measurement apparatus, shown in Figure 3, consists of a $25 \times 30 \times 30 \, \text{cm}^3$ tank that is filled with the diluted scattering medium. The depth of the tank is large enough to ensure the scattering angles are adequately covered (0 to 175 degrees). The volume of the tank is designed to be large enough to dilute concentrated media such as milk. Two sides of the tank are constructed using anti-reflection glass and the other sides using diffuse black coated acrylic. A small frosted (diffuse) glass bulb fixed to a side

---

[1]When crystals are dissolved in water, they may exhibit different scattering properties due to ionization.
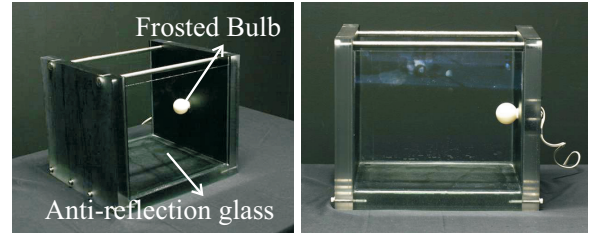

Figure 3: *Two views of the apparatus used to measure scattering properties of water-soluble media. A glass tank with rectangular cross-section is fitted with a small light bulb. The glass is anti-reflection coated. Different volumes of participating media are diluted with water in the tank, to simulate different concentrations. A camera views the front face of the tank at normal incidence to avoid refractions at the medium-glass-air boundaries.*
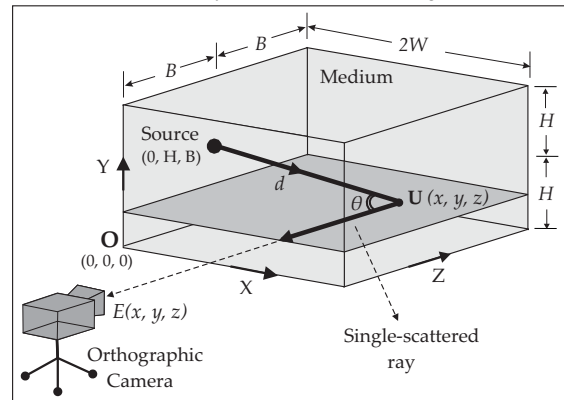

Figure 4: *A volume filled with a homogeneous participating medium and illuminated by an isotropic point light source. A camera views the front face of the volume at normal incidence. The path of one single-scattered ray as it travels from the source to the camera is shown. This ray is first attenuated in intensity over a distance d, is then scattered at an angle $\pi - \theta$, and finally, is attenuated again over a distance z, before reaching the camera. The irradiances due to all the rays that scatter into a viewing direction must be integrated to obtain the final camera irradiance.*

of the tank illuminates the medium. A Canon EOS-20D 12-bit 3504x2336 pixel digital camera with a zoom lens is placed five meters away from the tank and observes a face of the tank at normal incidence. The field of view occupied by the tank in the image is three degrees and is therefore approximately orthographic. Orthographic projection avoids the need for modeling refractions of light rays at the medium-glass-air interfaces. In all our experiments, about 25 different exposures (1/500s to 10s) were used to acquire HDR images.

3.2 Image Formation Model

Although the basic principles of single scattering are well known, the exact nature of the image formation model depends on the geometry of the volume and the locations of the source and the camera. Figure 4 illustrates the illumination and measurement geometry based on our acquisition setup. For simplicity, we will assume that the medium is illuminated by an isotropic point light source (later we extend the analysis to area sources) of intensity I_0 that is located at the coordinates $(0, B, H)$.

Consider the path of one single-scattered light ray (thick ray in Figure 4) in the medium as it travels from the source to the camera. This ray is first exponentially attenuated in intensity for a distance d. At location $\mathbf{U}$ (x, y, z), depending on the phase function P, a fraction of the light intensity is scattered at an angle $\pi - \theta$. Finally, the ray is attenuated again for a distance z, before it reaches the camera. Mathematically, the irradiance at the camera produced by

this ray is written as [Sun et al. 2005],

$$E(x,y,z) = \frac{I_0}{d^2} \cdot e^{-\sigma d} \cdot \beta \, P(g, \pi - \theta) \cdot e^{-\sigma z} \cdot$$

$$d = \sqrt{x^2 + (y-H)^2 + (z-B)^2} \ , \ \cos\theta = (z-B)/d \ (1)$$

Here, $P(g, \pi - \theta)$ is the Henyey-Greenstein (H-G) phase function, and β and σ are the scattering and extinction coefficients (Figure 2). Then, the total irradiance E at pixel (x,y) in the camera is obtained by integrating intensities due to all rays that are scattered at various angles along the pixel's line of sight (Z-direction),

$$E(x,y) = \int_0^{2B} E(x,y,z)\,dz$$

$$= \beta \int_0^{2B} \frac{I_0 \, e^{-\sigma(z + \sqrt{x^2+(y-H)^2+(z-B)^2})}}{x^2 + (y-H)^2 + (z-B)^2} \, P(g, \pi - \theta)\,dz. \quad (2)$$

The above equation relates the camera irradiances as a function of the three medium parameters, σ, β and g. Although obtaining an analytic (closed-form) solution to the above integral is hard [Sun et al. 2005], it is straightforward to evaluate it numerically.

3.3 Space of valid medium parameters

Different materials have their own natural densities and scattering properties, which are all unknown before experimentation. So, how do we know if single scattering is dominant at a particular concentration for a given material? Note that the scattering β, absorption κ and extinction σ, coefficients are proportional to the concentration (fraction of volume diluted in water) of the medium. Thus, we performed exhaustive simulations to derive the complete space of parameters for which the above image formation model is accurate[2]. For ground truth, we simulated the irradiances obtained using multiple scattering for the same set of parameter values, using a standard volumetric Monte Carlo technique. Figure 5 shows a plot of the differences between energies captured by the single scattering and multiple scattering simulations for a set of parameter values. From the RMS errors in the plot, we can define the upper bounds on the parameters κ and $\sigma = \beta + \kappa$ as those for which the energy differences between our model and the ground truth are less than five percent. For example, the valid domain where single scattering is dominant, is approximately $\sigma < 0.04$ for $\kappa < 0.004$.

3.4 How to choose the best concentration?

Based on the simulations, we present an experimental method to determine the best concentration for our measurements. Figure 6 shows images acquired of different concentrations of milk and MERLOT. Which among these images should we use to measure the scattering properties? Several heuristics may be used to decide on a particular concentration. For instance, the extent of blurring of the light source provides us a good clue to determine whether multiple scattering is significant (rightmost image in Figure 6). A better heuristic is to compute an approximation to the extinction coefficient σ from the attenuated brightness of the light source. Under single scattering, the radiance in the direction of the source (distance d) can be approximated using exponential attenuation as:

$$E(0) \approx \left(\frac{I_0}{d^2}\right) e^{-\hat{\sigma} d}, \quad (3)$$

---

[2]This extends the simulations in [Sun et al. 2005], where a small part of the possible parameter space (pure isotropic scattering) was considered.
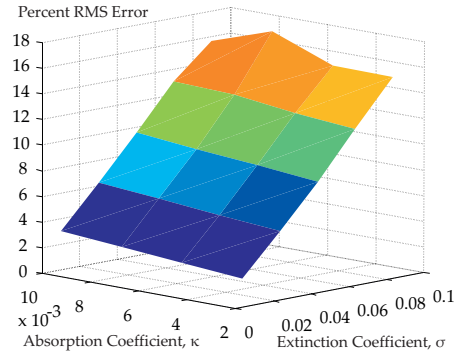

Figure 5: *Plot showing the differences between irradiances obtained by simulating single scattering and multiple scattering (ground truth) models, for a large space of parameter values σ and $\kappa = \sigma - \beta$. An upper bound on the differences of, say, 5%, can be used to define the range of parameters for which single scattering is a valid approximation. From the plot, the valid range is approximately $\sigma < 0.04$ for $\kappa < 0.004$.*

where $\hat{\sigma}$ is an estimate of the extinction coefficient σ. In the absence of multiple scattering, this estimate is closer to the true value of σ (and varies linearly with concentration), whereas, in the presence of multiple scattering, this estimate is called *diffuse or reduced attenuation coefficient* [Ishimaru 1978] and is usually much lesser than σ. Thus, we can determine whether the concentration can be used for measurement by observing the plot (Figure 7 of $\hat{\sigma}$ versus the volume fraction of the medium diluted with water). Figure 7 shows that after a certain amount of milk is added to water, the $\hat{\sigma}$ no longer remains linear with concentration (dashed line), and must not be used for measurements. For a purely absorbing liquid like wine (MERLOT), the plot is completely linear and any image that has the best signal-to-noise ratio may be used. Similarly, the plot shows that coke scatters, albeit weakly, and ESPRESSO coffee scatters light strongly. We use this simple procedure to try several concentrations and observe where the linearity in the plot fails to determine the best concentration. As a further test, we check if the estimated parameters from this concentration lie within the valid space of parameters simulated above.
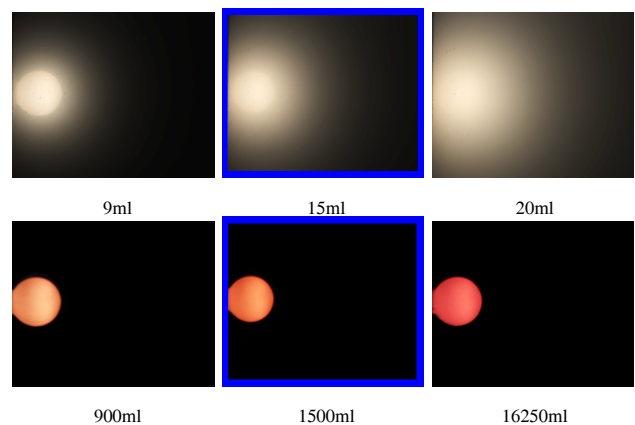

Figure 6: *Images illustrating different degrees of scattering and absorption. [Top row] Images of milk at various concentrations. Since milk is a highly scattering liquid, we observe an increase in blurring with increasing concentration. [Bottom Row] Images of red wine at various concentrations. Red wine is a highly absorbing liquid, showing only a saturation of the bulb color with increasing concentration, and no blurring. The highlighted images are chosen for estimating the parameters.*
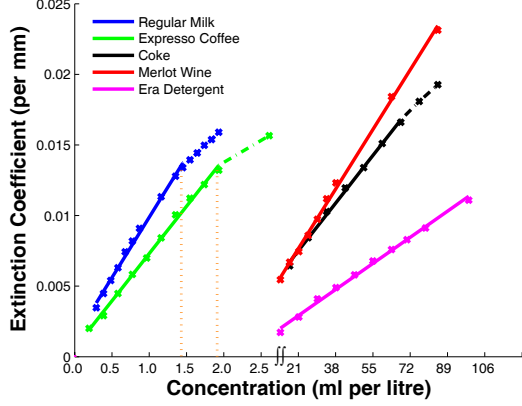
Figure 7: *Plot of extinction coefficient estimate $\hat{\sigma}$ as a function of the volume of the media diluted in water in the measurement apparatus. The plots are linear when multiple scattering is negligible and single scattering is dominant. As the concentrations of media (and hence multiple scattering) increase, the estimated $\hat{\sigma}$ is less than the true extinction coefficient σ. For a highly scattering medium such as milk, the linearity fails at very low concentrations, while for an absorbing medium such as MERLOT, the linearity is always preserved.*

4 Estimating Medium Properties based on Single Scattering

In this section, we present a non-linear minimization algorithm to estimate the properties of the medium (σ, β and g), from the measured image irradiances $E(x,y)$ (see Equation (2)). We then demonstrate the accuracy of the algorithm through extensive simulations.

4.1 Formulating the Error Function

The error at each pixel is written as the difference between the measured irradiance $E(x,y)$ and the irradiance predicted by the model in equation 2,

$$\mathscr{F}(x,y) = E(x,y) - RHS(x,y). \tag{4}$$

Here $RHS(x,y)$ is the numerically evaluated right hand side integral in the model of equation 2. Then, the parameters σ, β and g can be estimated by computing the global minimum of the sum of squares of the errors of all the pixels, as,

$$\min_{\beta,\sigma,g} \sum_y \sum_x \mathscr{F}^2(x,y). \tag{5}$$

The above function essentially requires a 3-parameter search. However, note that the parameter β is a global scale factor. Thus, we can eliminate β by defining a normalized error function as,

$$\mathscr{F}_{norm}(x,y) = \frac{E(x,y)}{\max\limits_{x,y} E(x,y)} - \frac{RHS(x,y)}{\max\limits_{x,y} RHS(x,y)}. \tag{6}$$

Now, instead of requiring a 3-parameter search, the above problem can be reduced to a 2-parameter search that minimizes the normalized objective function to estimate σ and g:

$$\min_{\sigma,g} \sum_y \sum_x \mathscr{F}^2{}_{norm}(x,y). \tag{7}$$

Then, the scale factor β can be recovered using the original function $\mathscr{F}$. To compute the global minimum, we use Nelder-Meade search implemented by the Matlab^{TM} function "fminsearch".
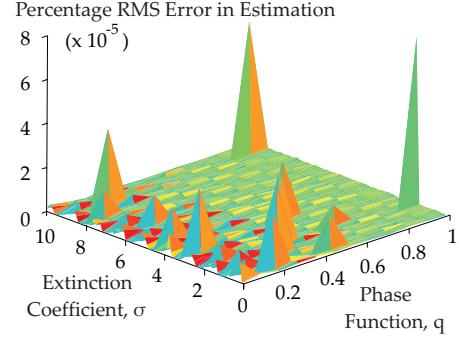

Figure 8: *Plot showing the errors in reconstruction of the single scattering parameters σ and $q = |g|$, where $-1 < g < 1$, compared to ground truth values. The low errors indicate the accuracy of our estimation technique. The maximum of the errors for positive or negative g is shown.*

4.2 Estimation Accuracy using Simulations

Fortunately, since the space of the possible parameters is small (see Section 3.3), exhaustive simulation of the above algorithm is possible. We only show the correctness of the estimated parameters σ and g, using Equation (7). The estimation of the scale factor β then follows trivially. Gaussian noise of unit standard deviation was added in all our simulations. The non-linear search was initialized randomly for both the parameters σ and g. The plot in Figure 8 shows the error in the estimated parameters as compared to ground truth values. In all the cases, the estimation errors were less than 0.0001%, and the number of iterations required for convergence was less than 100. Since the numerical evaluation of the integral is very fast, the time for convergence is usually of the order of a few minutes. This demonstrates that the inverse estimation is fast and results in unique and correct parameters.

4.3 Implementation Issues

We present two issues that need careful implementation for our algorithm to be successful on real images.

Calibrating the area source: Our method does not rely on isotropic point sources but requires only a calibrated divergent source to take advantage of the different phase angles measured in the same view and hence, any off-the-shelf bulb suffices. For our real setup, we have implemented a spherical diffuse area source. To compute the irradiance at any point P within the tank, we sample (using roughly 10x10 samples) the hemisphere of the bulb that is visible to that point P. The non-uniform directional intensities and intensity fall-off were calibrated carefully by using a light meter at discrete 3D locations within the tank. The camera also measures a pure water image (without any scattering or absorption) to give the image irradiance of each source element (sample). This irradiance along with the fall-off value and the pixel solid angle is used to determine the intensity without scattering.

Instabilities in the H-G phase function for highly absorbing media: The H-G phase function was designed for scattering media and is not defined for purely absorbing media. However, for highly absorbing media, the scattering coefficient β is very low and the average cosine $g \approx 1$ since rays only pass straight through, much like highly forward scattering media. Even though this was not a problem in simulations, the instability for $g > 0.95$ can be high in real experiments. For this special case, we simply use a truncated legendre polynomial expansion of the H-G phase function as $P(g,\theta) = \sum_i (2i+1) g^i L_i(\theta)$, and truncate to less than 100 terms. As an undesirable byproduct the fits may show some "ringing" at the tail of the phase function. However, this truncated function still fits higher brightness well and thus does not affect appearance strongly. Despite this instability, the H-G phase function is flexible enough to model the scattering behavior of all our materials.
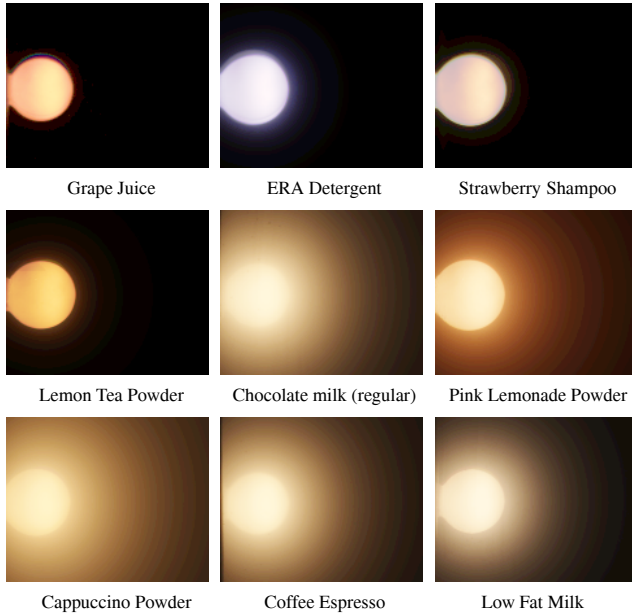
Figure 9: *Captured photographs of a variety of water-soluble media illustrating different degrees of scattering and absorption. For highly scattering media such as milk, chocolate milk and espresso, we observe a significant blur around the bulb. For highly absorbing media such as grape juice, there is very little scattering. All the images have wide dynamic range of intensities and hence, we have tone-mapped them for illustration.* **Please see supplementary material for more images.**

5 Actual Measurements and Validation

Using our approach, we have measured the scattering properties of a broad class of **forty** commonly found participating media that can be either (a) diluted in water such as juices (for example, apple, strawberry, orange), beverages (for example, coffee, soft drinks, milks, wines, beers), cleaning supplies (detergents), or (b) suspended in natural waters such as impurities and organisms, or even (c) dissolved in water such as powders and sugar, salt crystals. In addition to liquids available at the usual supermarkets, we have also collected four samples from different locations and depths in the Pacific ocean. We then present detailed validation by showing that our parameters extrapolate correctly to higher concentrations as well, where multiple scattering is prominent.

A subset of nine photographs of the diluted set of liquids contained in the glass tank is shown in Figure 9, similar to the four in Figure 1. Together, these include representative types of media such as highly scattering, highly absorbing and moderate levels of absorption and scattering. The images show a high dynamic range of brightness and are enhanced to show the scattering effects. The set of scattering parameters for all the media is shown in Table 1. The extinction (σ) and scattering (β) coefficients are given for each of the three color channels, red, green and blue. The phase function parameter g is also shown for the three color channels. Note that all the extinction and scattering coefficients are less than 0.04 in accordance with our simulations in Section 3.3. Also, as expected, in all cases, the scattering coefficient does not increase with wavelength.

5.1 Fits to Measured Brightness Profiles

We demonstrate the accuracy of our technique by reconstructing the photographs using the estimated parameters. Although we considered the brightness at all pixels in the captured photographs, for illustration purposes we show only the profile of intensity values in the direction that is radially outward from the source. Figure 10
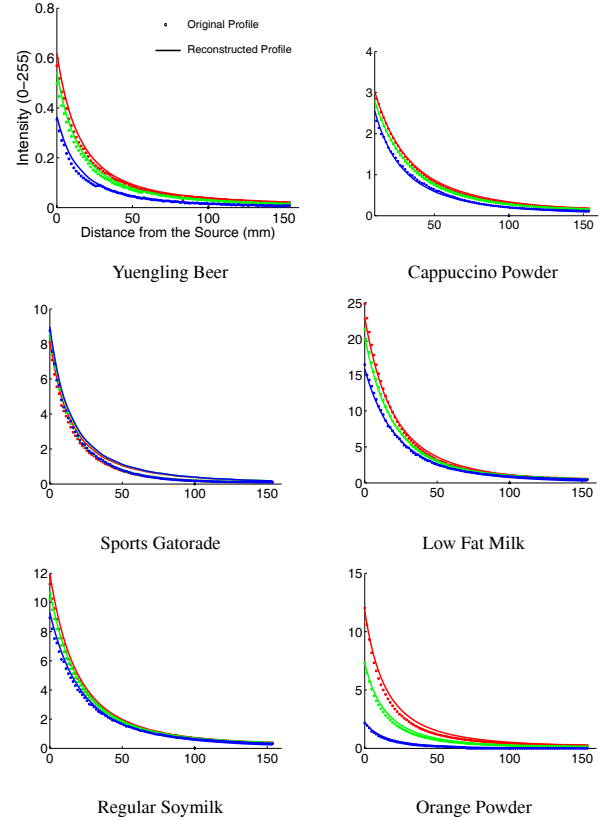

Figure 10: *Fits obtained using the estimated parameters as compared against the corresponding measured brightness profiles in the captured photographs. The brightness profile is measured radially outward from the source in the image. The red, green and blue plots correspond to the three color channels of the camera. The match between the estimated and measured data demonstrates the accuracy of the estimation technique. The fits for six (out of 40) representative materials with varying degrees of absorption and scattering are shown.* **Please see the supplementary material for more plots.**

shows the good fits obtained using the estimated parameters compared against the measured profiles for a subset of six materials of varying degrees of scattering and absorption properties (please review supplementary document for plots of other materials). When there is no scattering (pure absorption), fitting a scattering model can induce some "ringing" effect in the dark tail end of the profile. We can detect this special case and use the attenuation model to compute the absorption coefficient ($\kappa = \sigma$).

5.2 Extrapolation to higher concentrations

The extinction and scattering coefficients are proportional to the concentration of the medium. Thus, if β_1 and σ_1 are estimated at concentration c_1, then the coefficients β_2 and σ_2 at another concentration c_2 can be extrapolated using:

$$\beta_2 = \beta_1 \left(\frac{c_2}{c_1} \right) \; , \; \sigma_2 = \sigma_1 \left(\frac{c_2}{c_1} \right) . \qquad (8)$$

Note, however, that g is independent of the medium concentration. While we estimate the parameters from lower concentrations, it is important to ensure that the parameters can be scaled to any concentration (where multiple scattering cannot be ignored) to produce accurate scattering effects. We show an example validation using fits obtained in comparison to the measured brightness profiles of chocolate milk at various concentrations. Figure 11 shows the fits

Material Name	Volume	Extinction Coefficient (σ) ($\times 10^{-2}$ mm^{-1})			Scattering Coefficient (β) ($\times 10^{-2}$ mm^{-1})			Average Cosine (g)			% RMS Error
		R	G	B	R	G	B	R	G	B	
Milk (lowfat)	16ml	0.9126	1.0748	1.2500	0.9124	1.0744	1.2492	0.932	0.902	0.859	0.95
Milk (reduced)	18ml	1.0750	1.2213	1.3941	1.0748	1.2209	1.3931	0.819	0.797	0.746	1.27
Milk (regular)	15ml	1.1874	1.3296	1.4602	1.1873	1.3293	1.4589	0.750	0.714	0.681	1.56
Coffee (espresso)	8ml	0.4376	0.5115	0.6048	0.2707	0.2828	0.2970	0.907	0.896	0.880	1.90
Coffee (mint mocha)	6ml	0.1900	0.2600	0.3500	0.0916	0.1081	0.1460	0.910	0.907	0.914	2.00
Soy Milk (lowfat)	16ml	0.1419	0.1625	0.2740	0.1418	0.1620	0.2715	0.850	0.853	0.842	1.75
Soymilk (regular)	12ml	0.2434	0.2719	0.4597	0.2433	0.2714	0.4563	0.873	0.858	0.832	1.68
Chocolate Milk (lowfat)	10ml	0.4282	0.5014	0.5791	0.4277	0.4998	0.5723	0.934	0.927	0.916	1.04
Chocolate Milk (regular)	16ml	0.7359	0.9172	1.0688	0.7352	0.9142	1.0588	0.862	0.838	0.806	2.19
Soda (coke)	1600ml	0.7143	1.1688	1.7169	0.0177	0.0208	0.0000	0.965	0.972	−	4.86
Soda (pepsi)	1600ml	0.6433	0.9990	1.4420	0.0058	0.0141	0.0000	0.926	0.979	−	2.92
Soda (sprite)	15000ml	0.1299	0.1283	0.1395	0.0069	0.0089	0.0089	0.943	0.953	0.952	3.22
Sports Gatorade	1500ml	0.4009	0.4185	0.4324	0.2392	0.2927	0.3745	0.933	0.933	0.935	3.42
Wine (chardonnay)	3300ml	0.1577	0.1748	0.3512	0.0030	0.0047	0.0069	0.914	0.958	0.975	5.10
Wine (white zinfandel)	3300ml	0.1763	0.2370	0.2913	0.0031	0.0048	0.0066	0.919	0.943	0.972	5.49
Wine (merlot)	1500ml	0.7639	1.6429	1.9196	0.0053	0.0000	0.0000	0.974	−	−	4.56
Beer (budweiser)	2900ml	0.1486	0.3210	0.7360	0.0037	0.0069	0.0074	0.917	0.956	0.982	5.61
Beer (coorslight)	1000ml	0.0295	0.0663	0.1521	0.0027	0.0055	0.0000	0.918	0.966	−	4.89
Beer (yuengling)	2900ml	0.1535	0.3322	0.7452	0.0495	0.0521	0.0597	0.969	0.969	0.975	4.48
Detergent (Clorox)	1200ml	0.1600	0.2500	0.3300	0.1425	0.1723	0.1928	0.912	0.905	0.892	1.99
Detergent (Era)	2300ml	0.7987	0.5746	0.2849	0.0553	0.0586	0.0906	0.949	0.950	0.971	4.17
Apple Juice	1800ml	0.1215	0.2101	0.4407	0.0201	0.0243	0.0323	0.947	0.949	0.945	4.92
Cranberry Juice	1500ml	0.2700	0.6300	0.8300	0.0128	0.0155	0.0196	0.947	0.951	0.974	4.60
Grape Juice	1200ml	0.5500	1.2500	1.5300	0.0072	0.0000	0.0000	0.961	−	−	5.19
Ruby Grapefruit Juice	240ml	0.2513	0.3517	0.4305	0.1617	0.1606	0.1669	0.929	0.929	0.931	2.68
White Grapefruit Juice	160ml	0.3609	0.3800	0.5632	0.3513	0.3669	0.5237	0.548	0.545	0.565	2.84
Shampoo (balancing)	300ml	0.0288	0.0710	0.0952	0.0104	0.0114	0.0147	0.910	0.905	0.920	4.86
Shampoo (strawberry)	300ml	0.0217	0.0788	0.1022	0.0028	0.0032	0.0033	0.927	0.935	0.994	2.47
Head & Shoulders	240ml	0.3674	0.4527	0.5211	0.2791	0.2890	0.3086	0.911	0.896	0.884	1.91
Lemon Tea Powder	5tsp	0.3400	0.5800	0.8800	0.0798	0.0898	0.1073	0.946	0.946	0.949	2.83
Orange Powder	4tbsp	0.3377	0.5573	1.0122	0.1928	0.2132	0.2259	0.919	0.918	0.922	2.25
Pink Lemonade Powder	5tbsp	0.2400	0.3700	0.4500	0.1235	0.1334	0.1305	0.902	0.902	0.904	1.02
Cappuccino Powder	0.25tsp	0.2574	0.3536	0.4840	0.0654	0.0882	0.1568	0.849	0.843	0.926	0.67
Salt Powder	1.75cup	0.7600	0.8685	0.9363	0.2485	0.2822	0.3216	0.802	0.793	0.821	1.34
Sugar Powder	5cup	0.0795	0.1759	0.2780	0.0145	0.0162	0.0202	0.921	0.919	0.931	1.80
Suisse Mocha Powder	0.5tsp	0.5098	0.6476	0.7944	0.3223	0.3583	0.4148	0.907	0.894	0.888	1.33
Mission Bay Surface Water (1-2 hours)		3.3623	3.2929	3.2193	0.2415	0.2762	0.3256	0.842	0.865	0.912	2.48
Pacific Ocean Surface Water (1 hour)		3.3645	3.3158	3.2428	0.1800	0.1834	0.2281	0.902	0.825	0.914	2.57
Mission Bay 10ft deep Water (30 min)		3.4063	3.3410	3.2810	0.0990	0.1274	0.1875	0.726	0.820	0.921	5.10
Mission Bay 10ft deep Water (8 hours)		3.3997	3.3457	3.2928	0.1018	0.1033	0.1611	0.929	0.910	0.945	5.13

Table 1: Scattering properties for 40 different water-soluble materials estimated using our technique. The second column lists the volumes *V* of the materials dissolved in $23 - V$ litres of water to achieve the desired levels of dilution where single scattering is dominant. These parameters can be proportionately scaled to any other volume V_n, using a scale factor of V_n/V. The percentage RMS errors (obtained over all pixels) quantify the accuracy of fits achieved with the estimated parameters to the measured intensity profiles. Errors for all the highly scattering media are less than 3%. For low-scattering materials, the total intensity of profiles is relatively low, thus making the estimation more sensitive to noise. Even for such low-scattering media, the errors are less than $5 - 6\%$. The last four rows are the parameters for various ocean water samples at their original concentrations. The **time elapsed** between the collection of samples and the image acquisition is listed in the parentheses. Since the suspended particles in ocean water settle down with time, we observe a small decrease in scattering coefficients in the sample for which 8 hours had been elapsed as compared to the one which was imaged just 30 minutes after collection. Note that all the extinction and scattering coefficients are less than 0.04 in accordance with our simulations in Section 3.3. As expected, the scattering coefficients do not decrease with wavelength. The scattering albedos (ratio of scattering coefficients to the extinction coefficients) is much higher for the scattering media (milk, coffee, orange powder) as compared to the absorbing ones (coke, wine). For materials that have $\beta = 0$, the phase function parameter g is undefined. As seen from the values of g which are closer to 1, several media are predominantly forward scattering. The parameters for the milks match those in [Jensen et al. 2001] up to a scale factor (due to the different fat contents in the milks used), providing further support for our estimation.

in this validation experiment. First, we estimate the parameters from the photograph of only 8ml of chocolate milk diluted in water, where single scattering is dominant. In (a), we show the fit obtained compared against the measured intensity profile. However, for higher concentrations of 50ml, 100ml and 150ml, multiple scattering cannot be ignored. For these cases, we scaled the coefficients (σ and β) by factors of $\{50/8, 100/8, 150/8\}$ (see Equation 8) and use them in a standard volumetric Monte Carlo renderer that includes multiple scattering. The plots in (b) - (d) demonstrate the strong fits obtained. This demonstrates that our parameters are robust enough to be extrapolated to higher concentrations. In fact, we will show renderings of most of the liquids at their natural concentrations (Section 6) despite measuring the parameters at significantly dilute states.
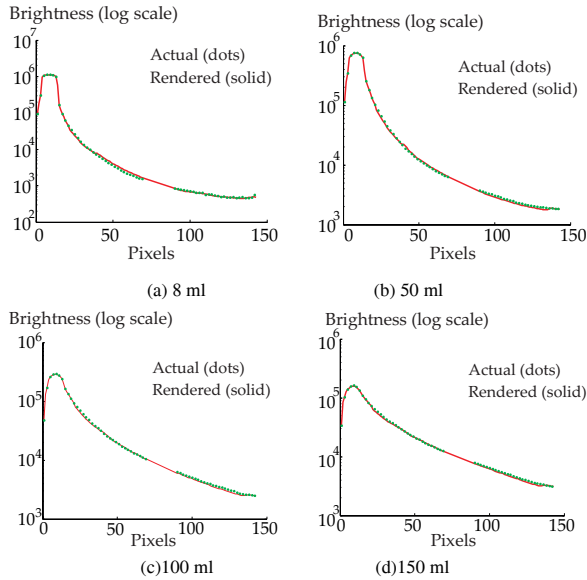
Figure 11: *Extrapolation of parameters to higher concentrations with multiple scattering. (a) 8 ml of chocolate milk is diluted in water and the parameters are estimated using the measured brightness profile. (b) - (d) The parameters estimated in (a) are scaled to higher concentrations (50ml, 100ml and 150ml) where multiple scattering cannot be ignored. Plots show a good fit between the brightness profile obtained by extrapolating our estimated parameters with a Monte Carlo renderer, and the ground truth measurements. The fits are shown in logarithmic scale.*

Figure 12: *Rendered scenes of liquids in a cognac glass under complex lighting. The KITCHEN environment map [Debevec 1998] was used for the lighting. The natural colors, shading and caustics indicate the high accuracy of our parameters.*
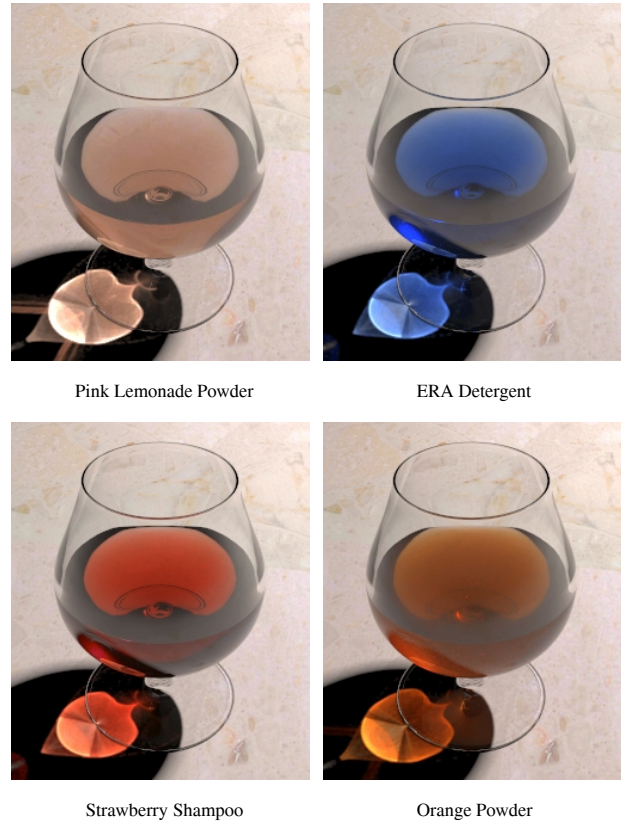

Figure 13: *Rendered scenes of liquids and powders in a cognac glass illuminated with a single directional white light source. The bright caustics show the colors transmitted through the media.*

6 Example Volumetric Renderings

The scattering properties estimated in this work can be input to any volumetric rendering algorithm to create visual effects of participating media. Here, we chose brute-force volumetric Monte-Carlo path tracing since it can be used to render arbitrary materials[3]. We use photon mapping for rendering caustics. For display purposes, we have applied a tone-mapping operator [Ward-Larson et al. 1997] to the renderings. Indices of refraction (IOR) of these media are also important for rendering. In initial experiments, we found the IOR to be between 1.33 (water) and 1.42 (milk) and varying linearly with concentrations, by using location of total internal reflection from the top of the water surface in the tank. In current renderings, we have simply used an IOR proportionate to the medium concentrations between 1.33 and 1.42, since this does not alter the visual appearance of the liquid drastically. We wish to perform thorough experiments in the future.

Figure 12 shows a mosaic of images of liquids rendered in their natural concentrations, partially filled in a cognac glass and illuminated by the "Kitchen Environment Map" [Debevec 1998]. These include two different types of wine (deep red MERLOT and golden-yellow CHARDONNAY), dark brown coffee ESPRESSO, and the golden-orange YUENGLING beer. Notice the color differences between MERLOT (no scattering) and ESPRESSO (moderate scattering) even though both of them are dark liquids. Observe that while beer and CHARDONNAY are very clear liquids, coffee is noticeably more opaque. Similarly, Figure 13 shows a mosaic of predominantly bright colored liquids such as the deep

---

[3]Under-sampling of path-traces can cause speckle noise seen in the renderings, and is not an artifact of our estimation.

| $\alpha = 0.03$ | $\alpha = 0.125$ | $\alpha = 0.25$ | $\alpha = 0.99$ |

| $\alpha = 0.03$ | $\alpha = 0.125$ | $\alpha = 0.25$ | $\alpha = 0.99$ |

Figure 14: *Effect of changing concentrations of a highly absorbing (MERLOT) and a highly scattering (milk) liquid. In the case of wine, notice that while the color gradually becomes deep red, the liquid remains clear, due to the lack of scattering. In the case of milk, however, we see a quick transition from a murky appearance to a soft white appearance, due to the high scattering albedo of milk.*

blue ERA detergent, the reddish strawberry shampoo, and powders dissolved in water such as the "pinkish" strawberry lemonade and orange powders. These images are illuminated only by a strong directional source to illustrate the bright caustics whose colorings are primarily due to absorption. We also present different types of novel visual effects obtained by changing or blending the parameters of different media to create realistic images of dilutions and mixtures of the original measured materials.

Effect of changing concentrations: Figure 14 illustrates the effects of changing concentrations of media in water. The top row shows a transition from pure water to MERLOT, obtained by scaling parameters of wine as in Equation 8. Notice the changes in caustics and the gradual deepening of the red color of the liquid. Note that as the transition occurs, the liquid remains clear even though the color changes; this is due to the pure absorbing nature of wine, as depicted by our parameters. The bottom row shows the effect of changing milk concentration in water. Since milk is a highly scattering medium, as expected, the appearance quickly changes from murky whitish water to soft and thick white milk. This is because the scattering albedo β/σ is high and the phase function parameter g is such that a significant amount of light diffuses into different directions.

Blending parameters for mixtures of media: For example, what are the properties of a mixture of ESPRESSO and milk, or otherwise known as *light coffee*? Consider a medium containing a mixture of two types of media, A and B. The properties of the individual media are denoted with the subscripts A and B. The scattering coefficient of the mixture is obtained by a weighted average,

$$\beta_{mix} = \frac{V_A \beta_A + V_B \beta_B}{V_A + V_B} .\qquad(9)$$

The absorption and extinction coefficients are similarly defined.

Unlike above where we just changed the scattering and absorption coefficients, here a new phase function parameter must be defined for the mixture as the weighted average [Key 2005],

$$g_{mix} = \frac{g_A \beta_A + g_B \beta_B}{\beta_{mix}} .\qquad(10)$$

These equations can be used to render mixtures of participating media or morph from one medium into another. Figure 15 shows mixing of different proportions of milk and wine. The second example shows a more common mixing of milk and coffee. Such mixing between materials, for the first time, gives a user the flexibility to create novel renderings of participating media.

7 Conclusion

Rendering the rich visual effects of participating media, like fluids or underwater impurities, requires precise measurements of their scattering properties. In this paper, we have developed a simple device and method for accurately estimating the scattering properties of a variety of media that can be diluted in water. Our approach only requires a single high dynamic range photograph. By diluting the medium, we work in the single scattering regime, where the inverse light transport problem is well conditioned—however, we can later render at arbitrary concentrations and even mix materials. We have presented a database of scattering parameters for 40 commonly found materials. This database is the first of its kind, and enables computer graphics practitioners to accurately render a wide variety of participating media, rather than having to set parameters in an ad-hoc fashion. In the future, we would like to improve this work by investigating different phase functions and measuring indices of refraction more accurately.

50% Milk + 50% Coffee   75% Milk + 25% Coffee

50% Wine + 50% Milk   75% Wine + 25% Milk

Figure 15: *Mixing two liquids - milk and coffee (top) and milk and wine (bottom), in different proportions. The wine-milk combination produces a soft pink appearance while the ESPRESSO-milk combination produces soft but brown appearance. (Minor noise due to Monte-Carlo under-sampling.)*

References

ANTYUFEEV, S. 2000. *Monte Carlo Method for Solving Inverse Problems of Radiative Transfer*. Inverse and Ill-Posed Problems Series, VSP Publishers.

BOSS, E., AND PEGAU, W. S. 2001. Relationship of light scattering at an angle in the backward direction to the backscattering coefficient. *Applied Optics 40 (30)*, 5503–5507.

CHANDRASEKHAR, S. 1960. *Radiative Transfer*. Oxford University Press.

DANA, K., NAYAR, S., VAN GINNEKEN, B., AND KOENDERINK, J. 1997. Reflectance and texture of real-world surfaces. In *Proc CVPR*, 151–157.

DEBEVEC, P. 1998. Rendering synthetic objects into real scenes: Bridging traditional and image-based graphics with global illumination and high dynamic range photography. *Proc. SIGGRAPH 98*, 189–198.

FINSY, E. G., AND JOOSTEN, J. 1991. Maximum entropy inversion of static light scattering data for the particle size distribution by number and volume. In *Advances in measurements and control of colloidal processes. Butterworth-Heineman, Ch. 30.*

FUCHS, E., AND JAFFE, J. S. 2002. Thin laser light sheet microscope for microbial oceanography. *OPTICS EXPRESS 10 (2)*, 145–154.

HAWKINS, T., EINARSSON, P., AND DEBEVEC, P. 2005. Acquisition of time-varying participating media. *ACM Trans. on Graphics (SIGGRAPH) 24*, 3, 812–815.

HENYEY, L., AND GREENSTEIN, J. 1941. Diffuse radiation in the galaxy. vol. 93, 70–83.

HULST, V. D. 1957. *Light Scattering by small Particles*. John Wiley and Sons.

ISHIMARU, A. 1978. *Wave Propagation and Scattering in Random Media. Volume 1: Single Scattering and Transport Theory*. Academic Press.

JAEGER, D., DEMEYERE, H., FINSY, R., SNEYERS, R., VANDERDEELEN, J., VAN-DER-MEEREN, P., AND VAN-LAETHEM, M. 1991. Particle sizing by photon correlation spectroscopy. part i: Monodisperse latices: influence of scattering angle and concentration of dispersed material. In *Part. Syst. Charact. 8, 179.*

JENSEN, H., MARSCHNER, S., LEVOY, M., AND HANRAHAN, P. 2001. A practical model for subsurface light transport. In *Proc. SIGGRAPH 01*, 511–518.

KEY, J. R. 2005. Streamer: User's guide. *Tech Report, NOAA/NESDIS, Madison, Wisconsin.*

MARSCHNER, S. 1998. Inverse rendering for computer graphics. *PhD Thesis, Cornell University.*

MATUSIK, W., PFISTER, H., BRAND, M., AND MCMILLAN, L. 2003. A data-driven reflectance model. *ACM Trans. on Graphics (SIGGRAPH) 22*, 3, 759–769.

MCCORMICK, N. J. 1981. A critique of inverse solutions to slab geometry transport problems. *Prog. Nucl. Energy 8.*

MCCORMICK, N. J. 1985. Sensitivity of multiple-scattering inverse transport methods to measurement errors. *JOSA A 2.*

MCCORMICK, N. J. 1996. Analytical transport theory applications in optical oceanography. *Annals of Nuclear Energy 23*, 381–395.

NARASIMHAN, S. G., AND NAYAR, S. K. 2003. Shedding light on the weather. In *CVPR 03*, 665–672.

OISHI, T. 1990. Significant relationship between the backward scattering coefficient of sea water and the scatterance at 120 degrees. *Applied Optics 29 (31)*, 4658–4665.

PRAHL, S. A. 1988. Light transport in tissue. *PhD Thesis, University of Texas at Austin.*

RAMAMOORTHI, R., AND HANRAHAN, P. 2001. A signal processing framework for inverse rendering. *Proc. SIGGRAPH 01*, 117–128.

SULLIVAN, S. A. 1963. Experimental study of the absorption in distilled water, artificial sea water, and heavy water in the visible region of the spectrum. *JOSA 53.*

SUN, B., RAMAMOORTHI, R., NARASIMHAN, S. G., AND NAYAR, S. K. 2005. A practical analytic single scattering model for real time rendering. *ACM Trans. on Graphics (SIGGRAPH) 24*, 3, 1040–1049.

WARD-LARSON, RUSHMEIER, H., AND PIATKO. 1997. A visibility matching tone reproduction operator for high dynamic range scenes. *IEEE Trans. on Visualization and Computer Graphics 3*, 4, 291–306.